Distribution and Radiative Forcing of Tropical Thin Cirrus Clouds

JOONSUK LEE

Cooperative Institute for Climate Studies, and Earth System Science Interdisciplinary Center, University of Maryland, College Park, College Park, Maryland

PING YANG AND ANDREW E. DESSLER

Department of Atmospheric Sciences, Texas A&M University, College Station, Texas

BO-CAI GAO

Naval Research Laboratory, Washington, D.C.

STEVEN PLATNICK

NASA Goddard Space Flight Center, Greenbelt, Maryland

(Manuscript received 20 April 2009, in final form 8 July 2009)

ABSTRACT

To understand the radiative impact of tropical thin cirrus clouds, the frequency of occurrence and optical depths of these clouds have been derived. ''Thin'' cirrus clouds are defined here as being those that are not detected by the operational Moderate Resolution Imaging Spectroradiometer (MODIS) cloud mask, corresponding to an optical depth value of approximately 0.3 or smaller, but that are detectable in terms of the cirrus reflectance product based on the MODIS 1.375-μm channel. With such a definition, thin cirrus clouds were present in more than 40% of the pixels flagged as ''clear sky'' by the operational MODIS cloud mask algorithm. It is shown that these thin cirrus clouds are frequently observed in deep convective regions in the western Pacific. Thin cirrus optical depths were derived from the cirrus reflectance product. Regions of significant cloud fraction and large optical depths were observed in the Northern Hemisphere during the boreal spring and summer and moved southward during the boreal autumn and winter. The radiative effects of tropical thin cirrus clouds were studied on the basis of the retrieved cirrus optical depths, the atmospheric profiles derived from the Atmospheric Infrared Sounder (AIRS) observations, and a radiative transfer model in conjunction with a parameterization of ice cloud spectral optical properties. To understand how these clouds regulate the radiation field in the atmosphere, the instantaneous net fluxes at the top of the atmosphere (TOA) and at the surface were calculated. The present study shows positive and negative net forcings at the TOA and at the surface, respectively. The positive (negative) net forcing at the TOA (surface) is due to the dominance of longwave (shortwave) forcing. Both the TOA and surface forcings are in a range of 0–20 W m^{-2}, depending on the optical depths of thin cirrus clouds.

1. Introduction

Numerous studies have demonstrated that thin cirrus clouds are frequently present near the tropical tropopause (Winker and Trepte 1998; McFarquhar et al. 2000; Massie et al. 2002; Pfister et al. 2001; Dessler et al. 2006). These clouds have been identified as one of the sources of uncertainty in the study of the earth's radiation budget and climate (Liou 1986; Lynch et al. 2002). Pfister et al. (2001) classified cirrus clouds into two types in terms of their formation mechanisms based on the analysis of temperatures along back trajectories run from these clouds. One type is thin quasi-laminar wisps cirrus associated with in situ formation by cooling of air on a synoptic scale or mesoscale; the second type is slightly lower, thicker, more structured cirrus originating from recent outflow of convection. Using the Halogen Occultation

Corresponding author address: Dr. Ping Yang, Dept. of Atmospheric Sciences, Texas A&M University, College Station, TX 77843.
E-mail: pyang@ariel.met.tamu.edu

DOI: 10.1175/2009JAS3183.1

Report Documentation Page

Form Approved
OMB No. 0704-0188

1. REPORT DATE	2. REPORT TYPE	3. DATES COVERED
JUL 2009		**00-00-2009 to 00-00-2009**

4. TITLE AND SUBTITLE	5a. CONTRACT NUMBER
Distribution and Radiative Forcing of Tropical Thin Cirrus Clouds	5b. GRANT NUMBER
	5c. PROGRAM ELEMENT NUMBER
6. AUTHOR(S)	5d. PROJECT NUMBER
	5e. TASK NUMBER
	5f. WORK UNIT NUMBER
7. PERFORMING ORGANIZATION NAME(S) AND ADDRESS(ES) **Naval Research Laboratory,4555 Overlook Avenue SW,Washington,DC,20375**	8. PERFORMING ORGANIZATION REPORT NUMBER
9. SPONSORING/MONITORING AGENCY NAME(S) AND ADDRESS(ES)	10. SPONSOR/MONITOR'S ACRONYM(S)
	11. SPONSOR/MONITOR'S REPORT NUMBER(S)

12. DISTRIBUTION/AVAILABILITY STATEMENT
Approved for public release; distribution unlimited

13. SUPPLEMENTARY NOTES

14. ABSTRACT
see report

15. SUBJECT TERMS

16. SECURITY CLASSIFICATION OF:			17. LIMITATION OF ABSTRACT	18. NUMBER OF PAGES	19a. NAME OF RESPONSIBLE PERSON
a. REPORT	b. ABSTRACT	c. THIS PAGE			
unclassified	**unclassified**	**unclassified**	**Same as Report (SAR)**	**12**	

Experiment (HALOE) observations, Massie et al. (2002) found that half the cirrus clouds observed during HALOE stemmed from convective blowoff, whereas the other half were associated with in situ formation.

Because of the high frequency of occurrence of thin cirrus clouds, the effect of these clouds on the earth's radiation budget can be significant. For example, these clouds, located high in the atmosphere, absorb longwave radiation but emit radiation at very low temperatures, producing local heating by a few degrees per day (Jensen et al. 1996; McFarquhar et al. 2000) and net positive cloud radiative forcing on the order of 1 W m^{-2} (Wang et al. 1996; McFarquhar et al. 2000). Because of the difficulties associated with in situ measurements, it is challenging to accurately quantify the radiative forcing of these clouds. To better understand the effect of thin cirrus clouds on climate, there is a pressing need to improve the current knowledge of the radiative effect of thin cirrus clouds near the tropopause.

Several studies based on lidar measurements (Winker and Trepte 1998; Pfister et al. 2001; Comstock et al. 2002) and ground-based measurements (Comstock and Sassen 2001; Mather et al. 1998; Platt et al. 1998) provided valuable results, but with temporal and spatial sampling limitations. The intent of this study is to understand the climatological characteristics of tropical thin cirrus optical depths, in particular those that are not detected by imagers using standard methods, and to quantify the radiative forcing of these clouds.

2. Data

A calculation of cloud radiative forcing requires cloud optical properties as well as the profiles of atmospheric water vapor and temperature. In this study, thin cirrus optical properties are derived from the operational Moderate Resolution Imaging Spectroradiometer (MODIS) cirrus reflectance dataset from the Earth Observing System (EOS) *Aqua* satellite. MODIS has 36 distinct spectral bands (20 reflected solar bands and 16 thermal emissive bands) with wavelengths ranging from 0.41 to 14.2 μm. In this study, level-2 cirrus reflectances (contained in the *Aqua* MODIS product MYD06) derived from the MODIS 0.66- and 1.375-μm band measurements (Gao et al. 2002) during a period from June 2005 to May 2006 are used to retrieve the corresponding cirrus optical depths. The retrieval is performed at every pixel between 30°S and 30°N latitudes, with a 1-km horizontal resolution. Additionally, level-2 cloud mask data (MYD35) are used to limit cirrus optical depth retrievals to those pixels identified as ''cloud free'' by the cloud mask. Recent studies suggest that the MODIS cloud mask has limited detection capability when cirrus optical depths are less than about 0.3 (Ackerman et al. 2008).

Measurements of tropospheric specific humidity (q) and temperature (T) are obtained from measurements made by the Atmospheric Infrared Sounder (AIRS) on *Aqua* (Aumann et al. 2003). The q and T data with an almost global coverage (Fetzer et al. 2006) have vertical resolutions of 2 and 1 km, respectively, and accuracies of 10% and 1 K, respectively. Sampling biases in the AIRS datasets are minimized by the retrieval ability of the instrument in the presence of up to 80% cloud cover (Susskind et al. 2003). The horizontal resolution of a single retrieval is 40–50 km.

3. Methodology

a. Optical depth of tropical thin cirrus clouds

Cirrus clouds are often present in the upper troposphere or lower stratosphere, and more than 90% of the total water vapor in the atmosphere is distributed beneath them (Gao and Kaufman 1995). In relatively humid environments, the MODIS 1.375-μm channel receives very little solar radiance reflected by the surface or the lower portion of the atmosphere (including low-level water clouds) when high-level cirrus clouds are not present. This is because the radiation within this band is absorbed by water vapor in the lower atmosphere under cirrus-free conditions. However, if high clouds are present, strong signals associated with the reflection and scattering of the incident solar radiation by these clouds are observed by the MODIS sensor at the 1.375-μm channel. Note that the reflected solar radiation observed by the MODIS sensor is slightly attenuated by water vapor above the clouds. The operational MODIS cirrus reflectance data product adjusts for this, determining the reflectance r_c that would exist in the absence of water vapor absorption (Gao et al. 2002).

This study focuses on tropical thin and subvisual cirrus clouds whose optical depths are quite small ($\ll 1$). In this case, the first-order scattering approximation is valid and the optical depth (τ) can be derived from the cirrus reflectance r_c as follows (Dessler and Yang 2003):

$$\tau = r_c \frac{4\mu\mu_0}{\tilde{\omega} P(\mu, \phi; -\mu_0\phi_0)}, \tag{1}$$

where μ is the cosine of the sensor zenith angle, μ_0 is the cosine of the solar zenith angle, ϕ is the sensor azimuthal angle, ϕ_0 is the solar azimuthal angle, $\tilde{\omega}$ is the single-scattering albedo, and P is the scattering phase function. The uncertainties of the retrieved optical thickness based on Eq. (1) due to the uncertainties in the phase function have been estimated by Dessler and Yang (2003).

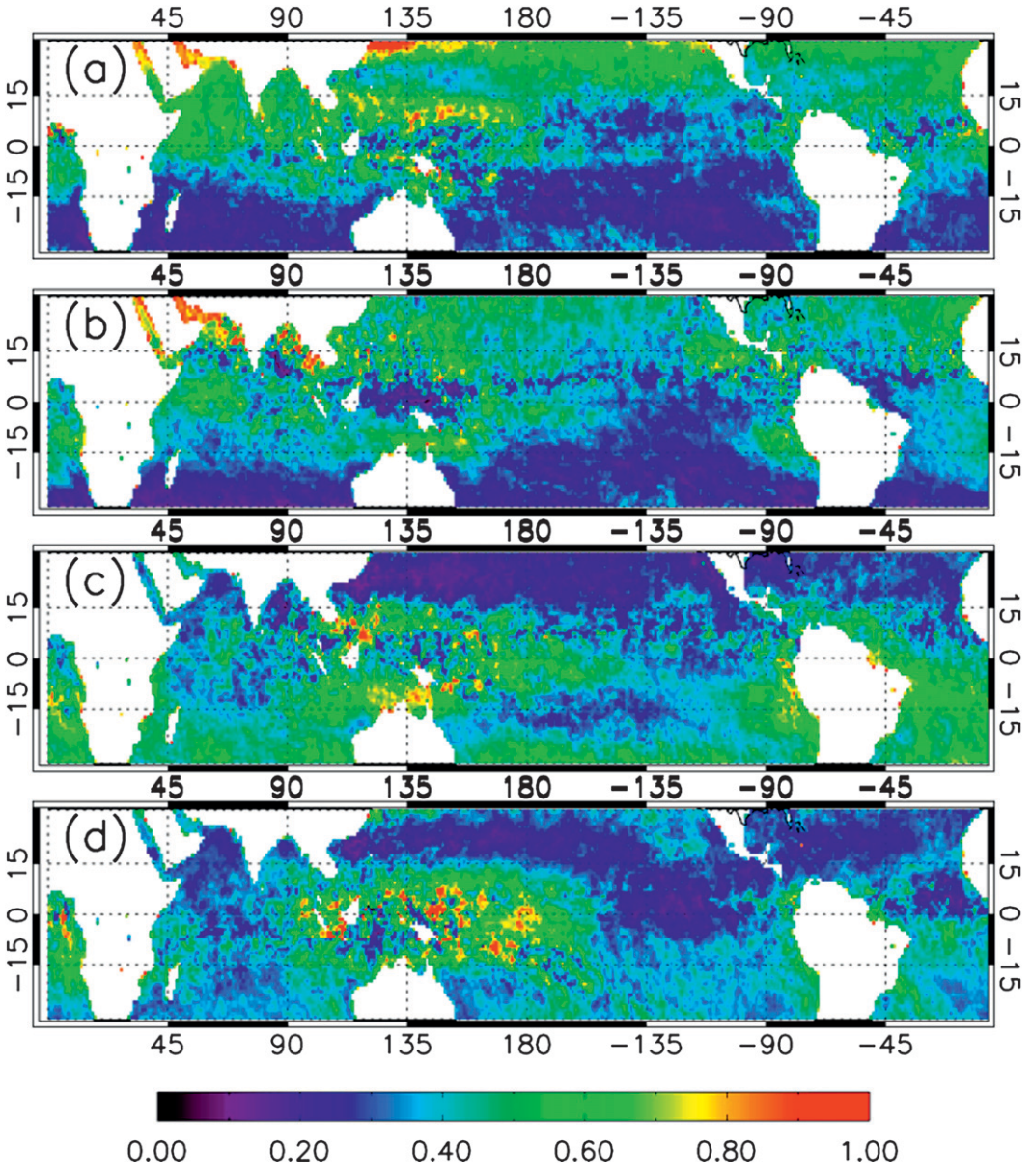

FIG. 1. Fraction of clear-sky observations for 1° × 1° boxes that have detectible thin cirrus optical depths larger than 0.02 for boreal (a) spring, (b) summer, (c) autumn, and (d) winter. The definition of season is determined by conventional boreal season such that spring months are March, April, and May; summer months are June, July, and August; autumn months are September, October, and November; and winter months are December, January, and February.

A method similar to the present approach has been developed by Meyer et al. (2004) using a rigorous radiative transfer model to generate lookup libraries for the τ–r_c relation, which includes the effect of multiple scattering and thus is applicable to both thin and thick cirrus clouds. However, the present method is more straightforward and computationally efficient although it is limited to thin and subvisual cirrus clouds. It should be noted that various complementary techniques have also been developed in the past two decades to derive cirrus microphysical and optical properties (e.g., Minnis et al. 1993a,b, 1995; King et al. 2004; Kokhanovsky and Nauss 2005; Chepfer et al. 1998, 2002; Stubenrauch et al. 1999), including the operational MODIS optical and microphysical cloud product (Platnick et al. 2003).

Ice crystals in cirrus clouds are nonspherical particles with complex shapes (e.g., Heymsfield 1975; Heymsfield and Iaquinta 2000). In the present retrieval, we assume

that a cirrus cloud consists of a mixture of bullet rosettes, hollow columns, aggregates, and hexagonal plates with percentages as follows: 25% plates, 25% hollow columns, and 50% bullet rosettes for size bins if the particle maximum dimension is smaller than 70 μm; and 20% plates, 20% hollow columns, 30% bullet rosettes, and 30% aggregates for size bins larger than 70 μm (Baum et al. 2000; Platnick et al. 2003; King et al. 2004). Specifically, the phase function used for the present retrieval of cirrus optical depth corresponds to an effective particle radius of 6.7 μm [see Fig. 4 in King et al. (2004); also see Kärcher and Lohmann (2002) and Garrett et al. (2003) for the size distribution of cirrus clouds], typical for cold cirrus clouds. The average cloud top pressure and temperature for the tropical thin cirrus clouds are 200 mb and 200 K (Pfister et al. 2001).

As noticed by Dessler and Yang (2003), the signals associated with the reflection of thin cirrus are quite weak. Thus, the reflection from a bright underlying surface under dry atmospheric conditions, such as over deserts where the radiation reflected by the surface is not completely absorbed by water vapor, may contaminate the signals associated with true cirrus reflection. For this reason, this study is confined to the cloud-free pixels over the oceans where the surface reflectance is relatively homogeneous and small. Dessler and Yang (2003) also analyzed various error sources and determined that the detection limit in terms of optical depth by this method is 0.02. If the retrieved optical depth is larger than 0.02 for a pixel, a thin cirrus cloud is assumed to be present within this pixel.

b. Radiative transfer model

To investigate the radiative forcing of thin cirrus clouds, the shortwave and longwave fluxes at the top of the atmosphere and at the surface are calculated from a radiative transfer model, namely LibRadtran developed by Mayer and Kylling (2005). The absorption of H_2O, O_2, O_3, CO_2, and N_2O is fully taken into account in the LibRadtran code. The profiles of temperature, H_2O, and O_3 are obtained from the AIRS level-3 monthly products. Using these profiles, background gaseous absorption properties are calculated using the correlated *k*-distribution method (Fu and Liou 1992, and references therein). Because the AIRS products do not provide atmospheric profiles at altitudes corresponding to pressures lower than 100 hPa for water vapor and 1 hPa for temperature, standard tropical atmospheric profiles are used above the highest AIRS levels. The distributions of other gases such as O_2, CO_2, and NO_2 are obtained from the standard tropical atmospheric profile. These profiles are interpolated into 100 layers in the model and cloud layer is inserted as one layer from 14 to 15 km.

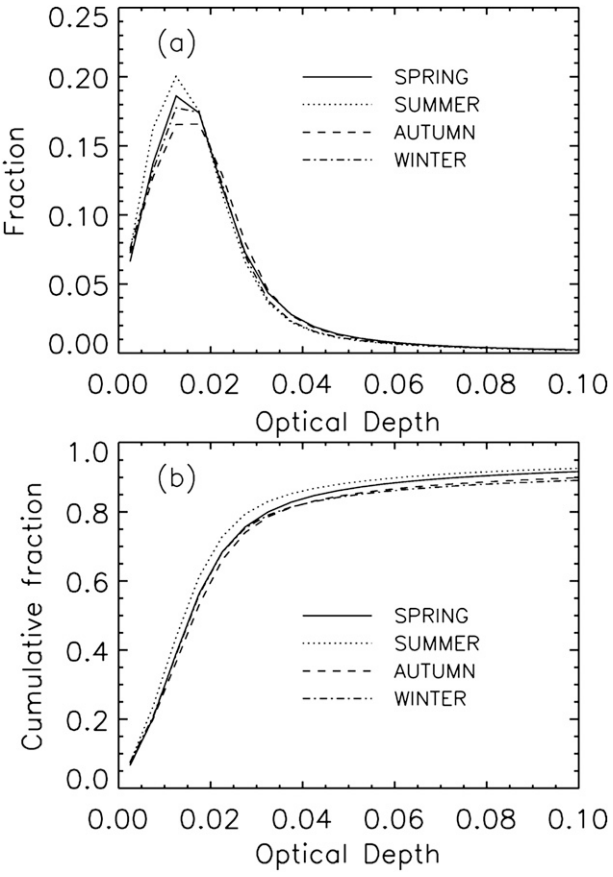

FIG. 2. (a) Histograms of optical depth of thin cirrus clouds retrieved between latitudes 30°S and 30°N for each of the boreal seasons. (b) Cumulative fractions of optical depth of thin cirrus clouds for each of the boreal seasons.

c. Bulk optical properties of ice clouds

The radiative properties of cirrus clouds are fundamentally determined by their microphysical and optical properties such as ice crystal shape, size distribution, ice water content (IWC), and effective particle radius (R_e). The single-scattering properties of ice clouds, namely the asymmetry parameter, extinction coefficient, and single-scattering albedo, are usually parameterized in terms of IWC and R_e.

In the past three decades, significant progress has been made in the parameterization of the bulk optical properties of ice clouds (e.g., Ebert and Curry 1992; Fu 1996; Fu et al. 1998; Key et al. 2002; McFarquhar et al. 2002; Edwards et al. 2007). The parameterization of cirrus optical properties in this study is based on that reported by Key et al. (2002) but with an extension to the infrared spectral band. Similar to Key et al. (2002), thirty size distributions reported by Fu (1996) and Mitchell et al. (1996) are used. The single-scattering properties of individual ice crystals are taken from Yang et al. (2000, 2005).

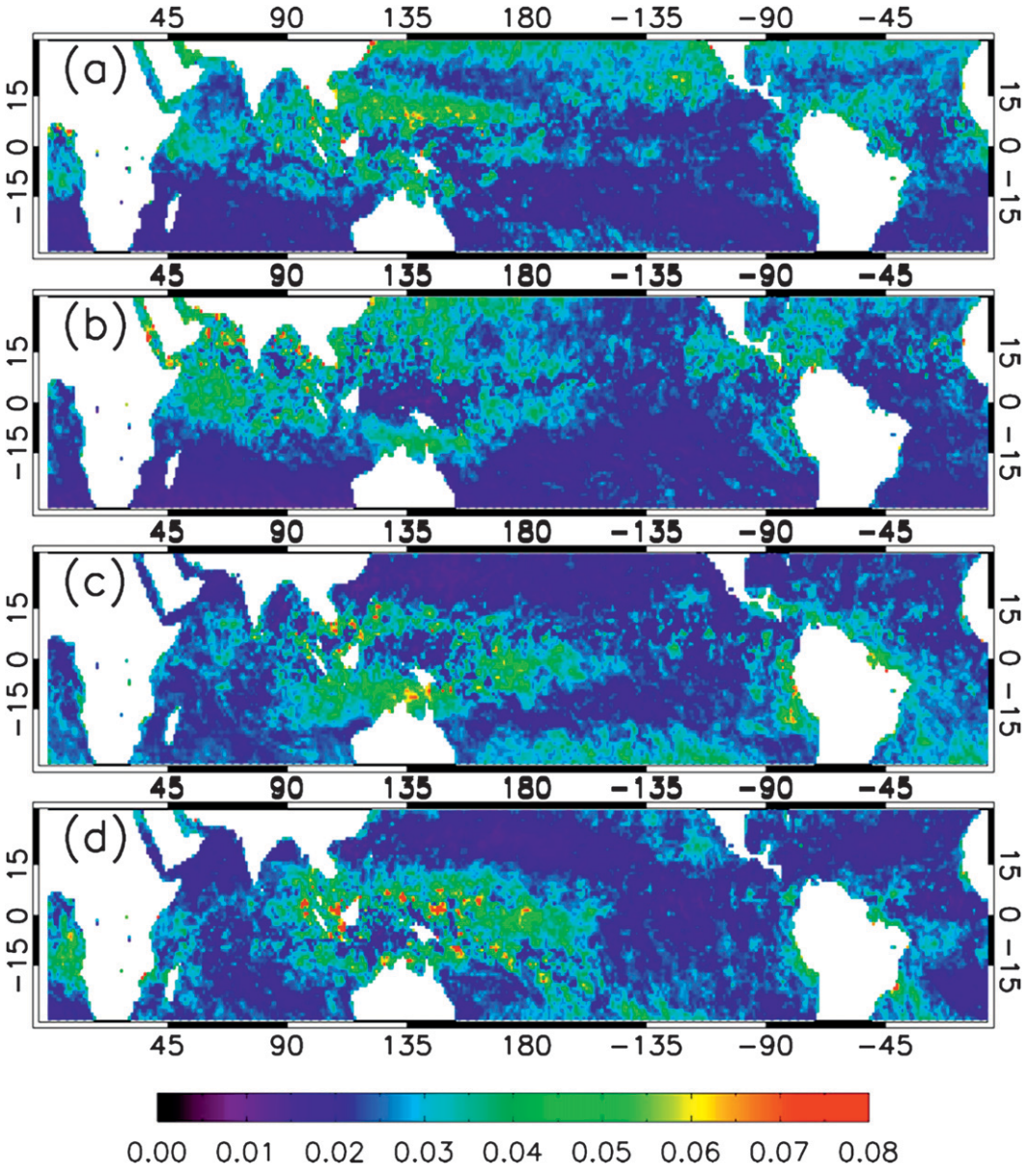

FIG. 3. Optical depth of tropical thin cirrus clouds for the pixels flagged as clear sky by MODIS for boreal (a) spring, (b) summer, (c) autumn, and (d) winter.

For computational efficiency in the simulation of radiation flux, a common approach is to approximate the scattering phase function in terms of the Henyey–Greenstein function (Henyey and Greenstein 1941). However, the Henyey–Greenstein function does not represent a good approximation to the true phase function in backscattering directions, particularly in the case of the phase functions of ice crystals. To overcome this shortcoming, in this study we follow Key et al. (2002) and use the double Henyey–Greenstein function. A method for determining the parameters involved in the double Henyey–Greenstein function has been reported by Key et al. (2002).

4. Results

a. The temporal and spatial distribution of tropical thin cirrus clouds

The temporal and spatial distributions of the mean optical depth of thin cirrus clouds and the frequency of occurrence are analyzed for a period from June 2005 to May 2006. The analysis is designed to determine the

locations of the maximum and minimum occurrences of thin cirrus clouds and to examine the characteristics of their seasonal variations.

Figure 1 shows the fraction of the MODIS observations made for clear-sky conditions according to the MODIS cloud mask, when optical depths obtained from Eq. (1) are larger than 0.02. Using ground-based lidar observation, Comstock et al. (2002) showed that the median optical depth of single layer cirrus clouds whose cloud-base heights are higher than 15 km is 0.019; that is, 50% of the optical depths of single-layer cirrus clouds measured by ground-based lidar are lower than 0.019. It is evident from Fig. 1 that high fraction occurs in the Northern Hemisphere during the boreal spring and summer and in the Southern Hemisphere during the boreal autumn and winter. In spring, the high fraction occurs over the western Pacific around Indonesia. The fraction is larger than 50% over most of the Northern Hemisphere oceans whereas the fraction is smaller than 30% over the Southern Hemisphere oceans. Over the western Pacific, the high fraction is observed around deep convection regions where thin cirrus clouds may be related to outflow from convective anvil cirrus or to in situ formation in the cold phase of waves spawned by the convection.

The fraction of observations for summer shows spatial distributions that are similar to those for spring. High fraction is observed over the western Pacific, the Persian Gulf, and Central America; low fraction occurs over the southeastern Pacific and the southern Indian Ocean. High fraction occurrences are still observed over the western Pacific but move southward in autumn. The Southern Hemisphere oceans show high fraction whereas the Northern Hemisphere oceans show less than 30% occurrence. Other high fraction regions are off the west coast of South America and off the west coast of southern Africa. The high fraction occurs over the western Pacific during winter and autumn and the low fraction is widely observed over Northern Hemisphere oceans.

Figure 2a shows the histograms of cirrus optical depths for each season. The seasonal fraction is calculated with a resolution of 0.005 for cirrus optical depth. The distributions for the four seasons are similar. For a given season, the fraction increases sharply to its maximum at optical depths near 0.01, decreases rapidly to small values at optical depths near 0.04, and further decreases at large optical depths to quite small values. Figure 2b shows the cumulative fraction of optical depth for each season. Using $\tau = 0.02$ as a detection limit as explained in section 3, 44%, 39%, 47%, and 44% of the observations flagged as cloud-free by the MODIS operational cloud mask algorithm have detectible thin cirrus clouds during the boreal spring, summer, autumn, and winter, respectively. Dessler and Yang (2003) showed that the percentage of detectible thin cirrus was 28% and 38% during the 6–8 June 2001 and 6–8 December 2000 periods, respectively. The percentage in the current study increased compared to that of Dessler and Yang (2003) during both seasons. The difference in the percentage between the two studies might result from the difference in the amount of analyzed data or from the fact that cloud formation increases in the afternoon. Note that the *Terra* MODIS data used in the study by Dessler and Yang (2003) were associated with morning properties whereas the *Aqua* MODIS data reflect afternoon properties. Using data from *Terra* and *Aqua* for the same period might be useful to understand the difference between morning and afternoon characteristics of thin cirrus clouds.

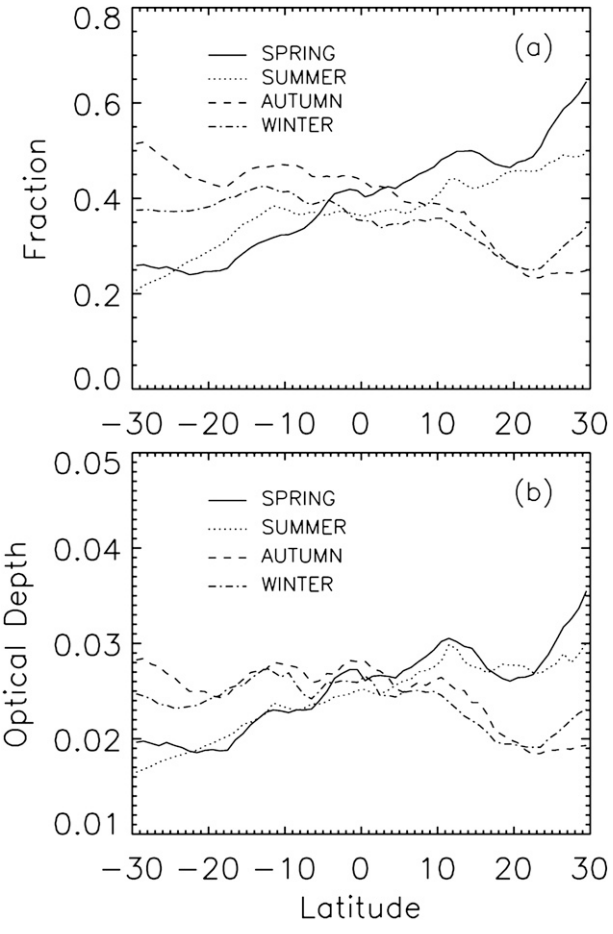

FIG. 4. Zonally averaged (a) fraction of observations and (b) optical depth of thin cirrus clouds for each season.

Figure 3 shows the spatial distributions of the average optical depths of tropical thin cirrus clouds for the pixels flagged as clear sky for each of the four seasons. The pattern is very similar to that of the observed fraction.

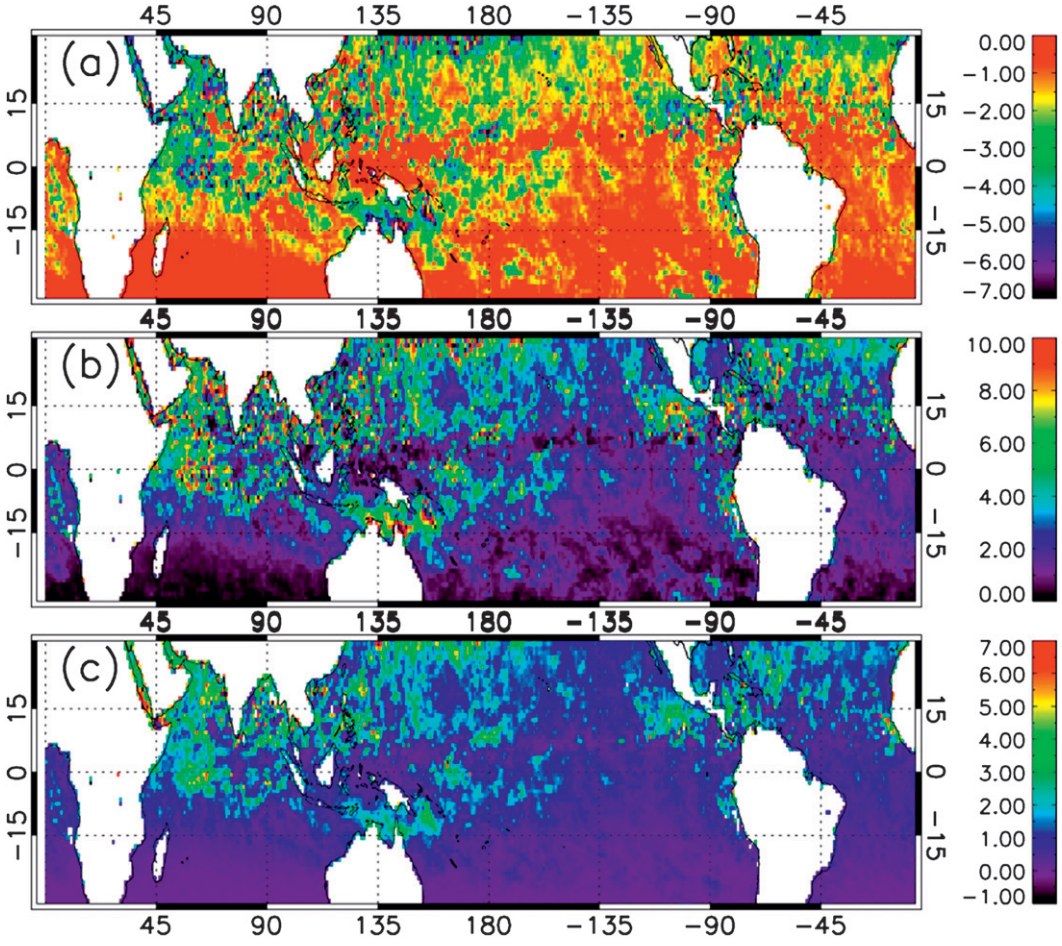

FIG. 5. Spatial distributions of (a) shortwave, (b) longwave, and (c) net cloud radiative forcing at the top of the atmosphere for June 2005. Units are W m^{-2}.

During spring, large optical depths are observed over the western and northern Pacific and small optical depths are observed over the Southern Hemisphere oceans. In summer, large optical depths appear widely over the western Pacific, the northern Indian Ocean, and Central America whereas small optical depths are observed over the Southern Hemisphere ocean areas. The locations of large optical depths are still observed over the western Pacific but migrate southward during autumn. Large optical depths also appear at the west coast of South America. The pattern of spatial distributions of optical depth for winter is similar to that for autumn when large optical depths are observed over the western Pacific and off the west coast of Africa.

Figure 4 shows the zonally averaged fraction of observations and optical depths. The fraction of observations and optical depths are averaged with a resolution of 1° over latitudes from 30°S to 30°N. From the figure, latitudinal variations of the fraction of observations and optical depths with the seasons are evident. The high fraction and large optical depths are observed in the Northern Hemisphere high latitudes and decrease toward the south during spring and summer. On the other hand, the high fraction and large optical depth appear in the Southern Hemisphere at high latitudes and decrease toward the north during autumn and winter.

b. The radiative forcing of thin cirrus clouds

Cloud radiative forcing has been investigated on the basis of satellite or ground-based measurements (e.g., Ramanathan et al. 1989; Rossow and Zhang 1995; Mace et al. 2006). Clouds have a warming effect on the surface or in the atmosphere by absorption and emission of longwave radiation and a cooling effect by reflecting the incident shortwave radiation. The net cloud radiative forcing is determined by the sum of longwave warming effect and shortwave cooling effect. The cloud radiative forcing is defined as the difference between clear conditions and all-sky conditions (Ramanathan et al. 1989; Hartmann et al. 2001; Yang et al. 2007).

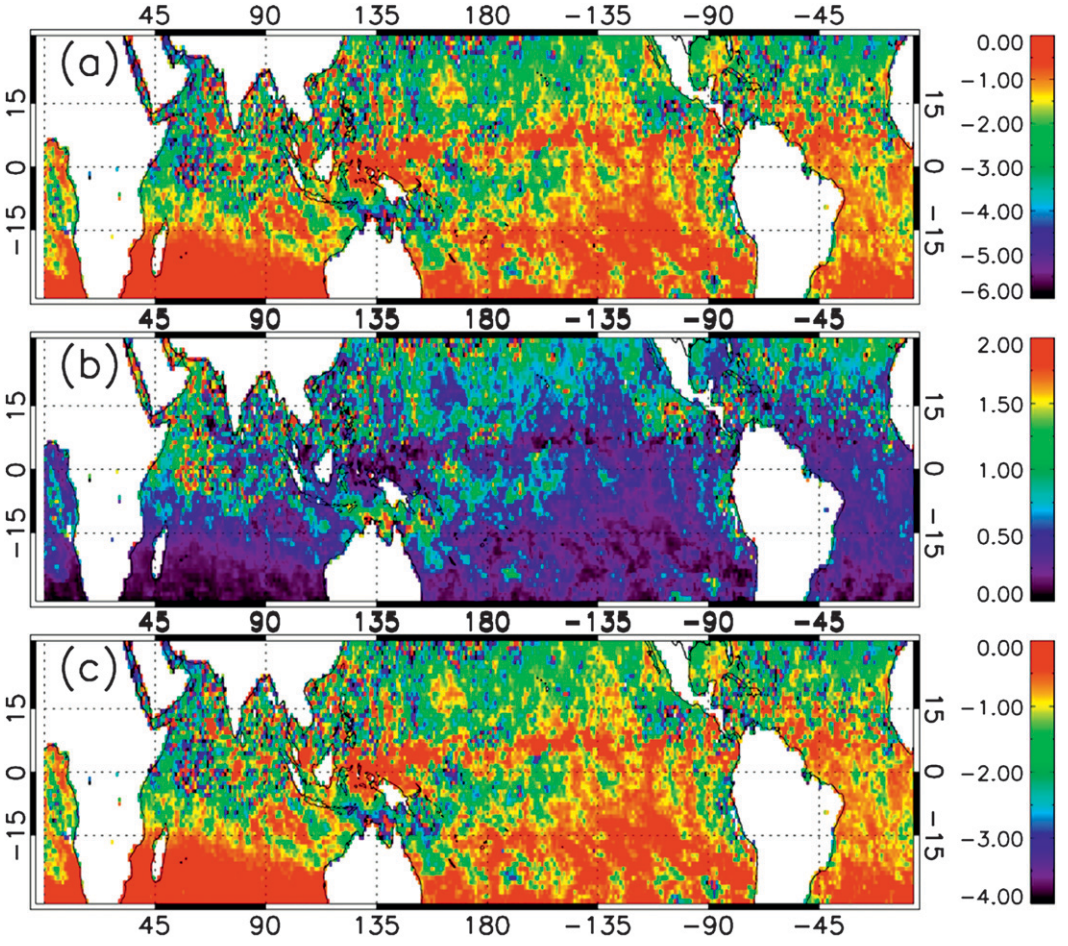

FIG. 6. As in Fig. 5, but at the surface for June 2005.

The solar zenith angle from each pixel is averaged over 1° × 1° latitude and longitude boxes for every month and is incorporated into the model calculation. Clear-sky fraction of observations with optical depths larger than 0.02 is used in the calculation of all-sky flux. Flux is calculated at each 1° × 1° box for each month using the monthly averaged optical depth, clear-sky fraction, solar zenith angle, and corresponding AIRS atmospheric profile.

Figure 5 shows the 1° × 1° spatial distribution of instantaneous cloud radiative forcing at the top of the atmosphere calculated from the retrieved optical depths, AIRS profile, and averaged solar zenith angle for June 2005. The large cloud radiative forcing appears around the western Pacific where the optical depths are large. It shows a negative cloud radiative forcing for shortwave radiation, a positive forcing for longwave radiation, and a net positive cloud radiative forcing.

Figure 6 shows the spatial distribution of instantaneous cloud radiative forcing at the surface for June 2005. Thin cirrus clouds produce large negative shortwave forcing in the Indian Ocean and the western Pacific Ocean but very small positive longwave forcing at the surface. Thus, the net cloud forcing shows a negative effect.

Figure 7 shows the relationship between optical depth and instantaneous cloud radiative forcing with respect to the solar zenith angle obtained from 1° × 1° calculations at the top of the atmosphere and at the surface. At the top of the atmosphere, both shortwave negative forcing and longwave positive forcing increase in magnitude with increasing optical depths. The net cloud radiative forcing shows positive values of 0–10 W m^{-2} because of larger positive longwave forcing. The difference in surface temperature and atmospheric profile causes the variation in the radiative forcing when the optical depth is constant.

At the surface, the radiative forcing of thin cirrus clouds is negative and positive for shortwave and longwave radiation, respectively, and the corresponding net forcing is in a range of −20 to 0 W m^{-2}. Shortwave negative forcing dominates at the surface. For overcast sky when the cloud fraction (N) is 1 (not shown here),

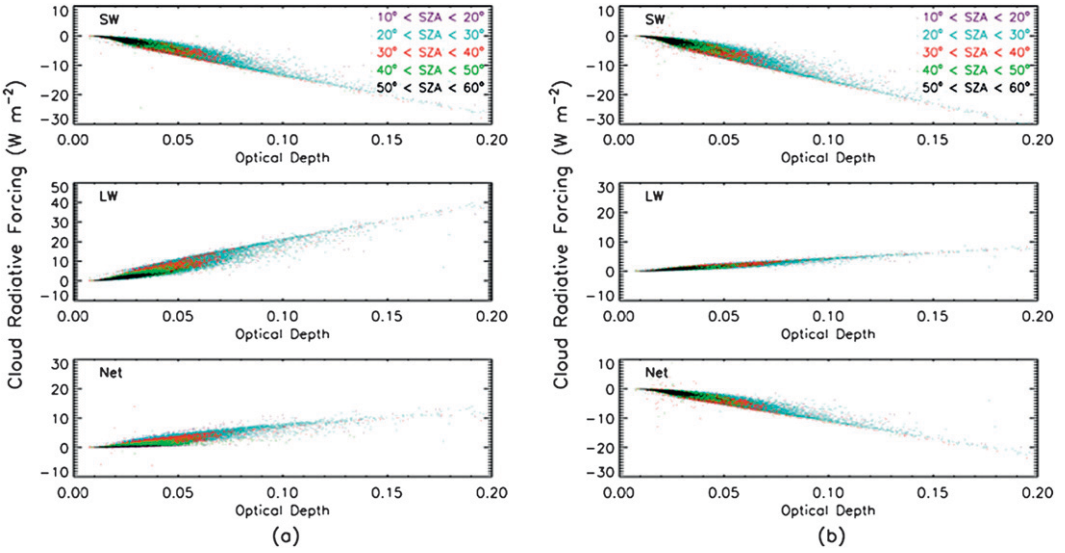

FIG. 7. (top) Shortwave, (middle) longwave, and (bottom) net cloud radiative forcing as a function of optical depth of thin cirrus clouds and solar zenith angle (a) at the top of the atmosphere and (b) at the surface.

the shortwave negative forcing increases in magnitude with the increasing solar zenith angle if the optical depth is the same. For longwave, the forcing does not depend on solar zenith angle. However, such a feature is not obvious after cloud fraction is incorporated into the radiative forcing calculation.

Table 1 lists the values of the seasonally averaged cloud radiative forcing between 30°S and 30°N. Thin cirrus clouds induce about 1 W m^{-2} net warming at the top of the atmosphere and 1.35 W m^{-2} net cooling at the surface. The possible contamination of clear-sky pixels by thin cirrus clouds may result in inaccuracies in the estimation of fluxes and atmospheric property retrievals. Further investigation is necessary to better understand those effects.

5. Summary

In this study, the frequency of occurrence of tropical thin cirrus clouds (defined here as those not detected by the operational MODIS cloud mask, corresponding to an approximate optical depth of about 0.3 or smaller), the mean optical depth, and the radiative impact were investigated. The optical depth of thin cirrus clouds were retrieved using the MODIS level-2 cirrus reflectance product. The retrieval was confined to clear-sky pixels over the oceans to remove the effect from the surface or lower atmosphere. Using $\tau = 0.02$ as a detection limit, over 40% of the observations flagged as cloud-free by MODIS have detectible thin cirrus clouds. The regions of high occurrence and large optical depth are located around deep convection areas and show seasonal variations. The thin cirrus clouds occur more frequently with larger optical depths in the Northern Hemisphere during spring and summer whereas they occur more frequently in the Southern Hemisphere during autumn and winter.

The instantaneous cloud radiative forcings at the top of atmosphere and at the surface are calculated to examine the radiative effect of this subset of thin cirrus clouds. The retrieved optical depth, fraction of observations, atmospheric profiles from AIRS, solar zenith angle, and parameterized single-scattering properties of ice clouds are used to simulate the radiative flux from the LibRadtran radiative transfer code. Thin cirrus clouds have a net positive radiative forcing at the top of atmosphere because of a larger positive longwave warming and a net negative radiative forcing at the surface because of a larger negative shortwave cooling. To improve current understanding of the properties of tropical thin cirrus clouds, accurate information about ice crystal particle size and cloud height may be necessary.

TABLE 1. The seasonal average of cloud radiative forcing between 30°S and 30°N latitudes. All units are W m^{-2}. (TOA is top of atmosphere; BOA is bottom of atmosphere.)

	Spring	Summer	Autumn	Winter
TOA SW	−1.74	−1.62	−1.79	−1.69
TOA LW	2.81	2.56	2.79	2.69
TOA NET	1.07	0.94	0.99	1.00
BOA SW	−2.01	−1.86	−2.06	−1.94
BOA LW	0.64	0.59	0.64	0.60
BOA NET	−1.37	−1.28	−1.41	−1.34

Acknowledgments. This research is supported by a research grant from NASA (NNX08AF68G) from the NASA Radiation Sciences Program managed by Dr. Hal Maring and the MODIS Program managed by Dr. Paula Bontempi. This study was also partly supported by a National Science Foundation (NSF) CAREER Award research grant (ATM-0239605).

REFERENCES

Ackerman, S. A., R. E. Holz, R. Frey, E. W. Eloranta, B. C. Maddux, and M. McGill, 2008: Cloud detection with MODIS. Part II: Validation. *J. Atmos. Oceanic Technol.,* **25,** 1073–1086.

Aumann, H. H., and Coauthors, 2003: AIRS/AMSU/HSB on the *Aqua* mission: Design, science objectives, data products, and processing systems. *IEEE Trans. Geosci. Remote Sens.,* **41,** 253–264.

Baum, B. A., D. P. Kratz, P. Yang, S. C. Ou, Y. Hu, P. F. Soulen, and S.-C. Tsay, 2000: Remote sensing of cloud properties using MODIS airborne simulator imagery during SUCCESS. I. Data and models. *J. Geophys. Res.,* **105,** 11 767–11 780.

Chepfer, H., G. Brogniez, and Y. Fouquart, 1998: Cirrus clouds' microphysical properties deduced from POLDER observations. *J. Quant. Spectrosc. Radiat. Transfer,* **60** (3), 375–390.

——, P. Minnis, D. Young, L. Nguyen, and R. F. Arduini, 2002: Estimation of cirrus cloud effective ice crystal shapes using visible reflectances from dual-satellite measurements. *J. Geophys. Res.,* **107,** 4730, doi:10.1029/2000JD000240.

Comstock, J. M., and K. Sassen, 2001: Retrieval of cirrus cloud radiative and backscattering properties using combined lidar and infrared radiometer (LIRAD) measurements. *J. Atmos. Oceanic Technol.,* **18,** 1658–1673.

——, T. P. Ackerman, and G. G. Mace, 2002: Ground-based lidar and radar remote sensing of tropical cirrus clouds at Nauru Island: Cloud statistics and radiative impacts. *J. Geophys. Res.,* **107,** 4714, doi:10.1029/2002JD002203.

Dessler, A. E., and P. Yang, 2003: The distribution of tropical thin cirrus clouds inferred from *Terra* MODIS data. *J. Climate,* **16,** 1241–1247.

——, S. P. Palm, W. D. Hart, and J. D. Spinhirne, 2006: Tropopause-level thin cirrus coverage revealed by ICESat/Geoscience Laser Altimeter System. *J. Geophys. Res.,* **111,** D08203, doi:10.1029/2005JD006586.

Ebert, E. E., and J. A. Curry, 1992: A parameterization of ice cloud optical properties for climate models. *J. Geophys. Res.,* **97,** 3831–3836.

Edwards, J. M., S. Havemann, J.-C. Thelen, and A. J. Baran, 2007: A new parametrization for the radiative properties of ice crystals: Comparison with existing schemes and impact in a GCM. *Atmos. Res.,* **83,** 19–35.

Fetzer, E. J., B. H. Lambrigtsen, A. Eldering, H. H. Aumann, and M. T. Chahine, 2006: Biases in total precipitable water vapor climatologies from Atmospheric Infrared Sounder and Advanced Microwave Scanning Radiometer. *J. Geophys. Res.,* **111,** D09S16, doi:10.1029/2005JD006598.

Fu, Q., 1996: An accurate parameterization of the solar radiative properties of cirrus clouds for climate models. *J. Climate,* **9,** 2058–2082.

——, and K.-N. Liou, 1992: On the correlated *k*-distribution method for radiative transfer in nonhomogeneous atmospheres. *J. Atmos. Sci.,* **49,** 2139–2156.

——, P. Yang, and W. B. Sun, 1998: An accurate parameterization of the infrared radiative properties of cirrus clouds for climate models. *J. Climate,* **11,** 2223–2237.

Gao, B.-C., and Y. J. Kaufman, 1995: Selection of 1.375-μm MODIS channel for remote sensing of cirrus clouds and stratospheric aerosols from space. *J. Atmos. Sci.,* **52,** 4231–4237.

——, P. Yang, W. Han, R.-R. Li, and W. J. Wiscombe, 2002: An algorithm using visible and 1.38-μm channels to retrieve cirrus clouds reflectances from aircraft and satellite data. *IEEE Trans. Geosci. Remote Sens.,* **40,** 1659–1668.

Garrett, T. J., H. Gerber, D. G. Baumgardner, C. H. Twohy, and E. M. Weinstock, 2003: Small, highly reflective ice crystals in low-latitude cirrus. *Geophys. Res. Lett.,* **30,** 2132, doi:10.1029/2003GL018153.

Hartmann, D. L., L. A. Moy, and Q. Fu, 2001: Tropical convection and energy balance at the top of the atmosphere. *J. Climate,* **14,** 4495–4511.

Henyey, L. G., and J. L. Greenstein, 1941: Diffuse radiation in the galaxy. *Astrophys. J.,* **93,** 70–83.

Heymsfield, A. J., 1975: Cirrus uncinus generating cells and the evolution of cirriform clouds. Part I: Aircraft observations of the growth of the ice phase. *J. Atmos. Sci.,* **32,** 799–808.

——, and J. Iaquinta, 2000: Cirrus crystal terminal velocities. *J. Atmos. Sci.,* **57,** 916–938.

Jensen, E. J., O. B. Toon, H. B. Selkirk, J. D. Spinhirne, and M. R. Schoeberl, 1996: On the formation and persistence of subvisible cirrus clouds near the tropical tropopause. *J. Geophys. Res.,* **101,** 21 361–21 375.

Kärcher, B., and U. Lohmann, 2002: A parameterization of cirrus cloud formation: Homogeneous freezing including effects of aerosol size. *J. Geophys. Res.,* **107,** 4698, doi:10.1029/2001JD001429.

Key, J. R., P. Yang, B. A. Baum, and S. L. Nasiri, 2002: Parameterization of shortwave ice cloud optical properties for various particle habits. *J. Geophys. Res.,* **107,** 4181, doi:10.1029/2001JD000742.

King, M. D., S. Platnick, P. Yang, G. T. Arnold, M. A. Gray, J. C. Riedi, S. A. Ackerman, and K.-N. Liou, 2004: Remote sensing of liquid water and ice cloud optical thickness, and effective radius in the Arctic: Application of air-borne multispectral MAS data. *J. Atmos. Oceanic Technol.,* **21,** 857–875.

Kokhanovsky, A. A., and T. Nauss, 2005: Satellite based retrieval of ice cloud properties using a semianalytical algorithm. *J. Geophys. Res.,* **110,** D19206, doi:10.1029/2004JD005744.

Liou, K.-N., 1986: Influence of cirrus clouds on weather and climate processes: A global perspective. *Mon. Wea. Rev.,* **114,** 1167–1199.

Lynch, D. K., K. Sassen, D. O. Starr, and G. Stephens, Eds., 2002: *Cirrus*. Oxford University Press, 480 pp.

Mace, G. G., S. Benson, and S. Kato, 2006: Cloud radiative forcing at the Atmospheric Radiation Measurement Program Climate Research Facility: 2. Vertical redistribution of radiant energy by clouds. *J. Geophys. Res.,* **111,** D11S91, doi:10.1029/2005JD005922.

Massie, S., A. Gettleman, W. Randel, and D. Baumgardner, 2002: Distribution of tropical cirrus in relation to convection. *J. Geophys. Res.,* **107,** 4591, doi:10.1029/2001JD001293.

Mather, J. H., T. P. Ackerman, M. P. Jensen, and W. E. Clements, 1998: Characteristics of the atmospheric state and the surface radiation budget at the tropical western Pacific ARM site. *Geophys. Res. Lett.,* **25,** 4513–4516.

Mayer, B., and A. Kylling, 2005: Technical note: The LibRadtran software package for radiative transfer calculations—Description and examples of use. *Atmos. Chem. Phys.,* **5,** 1855–1877.

McFarquhar, G. M., A. J. Heymsfield, J. Spinhirne, and B. Hart, 2000: Thin and subvisual tropopause tropical cirrus: Observations and radiative impacts. *J. Atmos. Sci.,* **57,** 1841–1853.

——, P. Yang, A. Macke, and A. J. Baran, 2002: A new parameterization of single scattering solar radiative properties for tropical anvils using observed ice crystal size and shape distributions. *J. Atmos. Sci.,* **59,** 2458–2478.

Meyer, K., P. Yang, and B.-C. Gao, 2004: Optical thickness of tropical cirrus clouds derived from the MODIS 0.66 and 1.38-μm channels. *IEEE Trans. Geosci. Remote Sens.,* **42,** 833–841.

Minnis, P., K.-N. Liou, and Y. Takano, 1993a: Inference of cirrus cloud properties using satellite-observed visible and infrared radiances. Part I: Parameterization of radiance fields. *J. Atmos. Sci.,* **50,** 1279–1304.

——, P. W. Heck, and D. F. Young, 1993b: Inference of cirrus cloud properties using satellite-observed visible and infrared radiances. Part II: Verification of theoretical cirrus radiative properties. *J. Atmos. Sci.,* **50,** 1305–1322.

——, and Coauthors, 1995: Cloud optical property retrieval (subsystem 4.3). Clouds and the Earth's Radiant Energy System (CERES) Algorithm Theoretical Basis Document, Volume III: Cloud Analyses and Radiance Inversions (Subsystem 4), NASA RP 1376, Vol. 3, 135–176.

Mitchell, D. L., S. K. Chai, Y. Liu, A. J. Heymsfield, and Y. Dong, 1996: Modeling cirrus clouds. Part I: Treatment of bimodal size spectra and case study analysis. *J. Atmos. Sci.,* **53,** 2952–2966.

Pfister, L., and Coauthors, 2001: Aircraft observation of thin cirrus clouds near the tropical tropopause. *J. Geophys. Res.,* **106,** 9765–9786.

Platnick, S., M. D. King, S. A. Ackerman, W. P. Menzel, B. A. Baum, J. C. Riedi, and R. A. Frey, 2003: The MODIS cloud products: algorithms and examples from *Terra*. *IEEE Trans. Geosci. Remote Sens.,* **41,** 459–473.

Platt, C. M. R., S. A. Young, P. J. Manson, G. R. Patterson, S. C. Marsden, R. T. Austin, and J. H. Churnside, 1998: The optical properties of equatorial cirrus from observations in the ARM Pilot Radiation Observation Experiment. *J. Atmos. Sci.,* **55,** 1977–1996.

Ramanathan, V., R. D. Cess, E. F. Harrison, P. Minnis, B. R. Barkstrom, E. Ahmad, and D. Hartmann, 1989: Cloud-radiative forcing and climate: Results from the Earth Radiation Budget Experiment. *Science,* **243,** 57–63.

Rossow, W. B., and Y.-C. Zhang, 1995: Calculation of surface and top of atmosphere radiative fluxes from physical quantities based on ISCCP data sets. 2. Validation and first results. *J. Geophys. Res.,* **100,** 1167–1198, doi:10.1029/94JD02746.

Stubenrauch, C. J., R. Holz, A. Chédin, D. L. Mitchell, and A. J. Baran, 1999: Retrieval of cirrus ice crystal sizes from 8.3 and 11.1 μm emissivities determined by the improved initialization inversion of TIROS-N Operational Vertical Sounder observations. *J. Geophys. Res.,* **104,** 31 793–31 808.

Susskind, J., C. D. Barnet, and J. M. Blaisdell, 2003: Retrieval of atmospheric and surface parameters from AIRS/AMSU/HSB data in the presence of clouds. *IEEE Trans. Geosci. Remote Sens.,* **41,** 390–409.

Wang, P.-H., P. Minnis, M. P. McCormick, G. S. Kent, and K. M. Skeens, 1996: A 6-year climatology of cloud occurrence frequency from Stratospheric Aerosol and Gas Experiment II observations (1985–1990). *J. Geophys. Res.,* **101,** 29 407–29 429.

Winker, D. M., and C. R. Trepte, 1998: Laminar cirrus observed near the tropical tropopause by LITE. *Geophys. Res. Lett.,* **25,** 3351–3354.

Yang, P., K.-N. Liou, K. Wyser, and D. Mitchell, 2000: Parameterization of the scattering and absorption properties of individual ice crystals. *J. Geophys. Res.,* **105,** 4699–4718.

——, H. Wei, H.-L. Huang, B. A. Baum, Y. X. Hu, G. W. Kattawar, M. I. Mishchenko, and Q. Fu, 2005: Scattering and absorption property database for nonspherical ice particles in the near-through far-infrared spectral region. *Appl. Opt.,* **44,** 5512–5523.

——, L. Zhang, G. Hong, S. L. Nasiri, B. A. Baum, H.-L. Huang, M. D. King, and S. Platnick, 2007: Differences between collection 4 and 5 MODIS ice cloud optical/microphysical products and their impact on radiative forcing simulations. *IEEE Trans. Geosci. Remote Sens.,* **45,** 2886–2899.